Research in Astronomy and Astrophysics, 23:095008 (12pp), 2023 September https://doi.org/10.1088/1674-4527/acd169

Large Telescope Wind Load Estimation with Gradient Segments Superposition and its Servo Control

Jia-Heng Yu[1], Song Xue[1,2,6], Tian Luan[1], Long-Yang Wang[1], Pei-Yuan Lian[1], Yue-Fei Yan[2,6], De-Qing Kong[3], Wu-Lin Zhao[4], Qian Xu[5], and Cong-Si Wang[2]

[1] School of Mechano-Electronic Engineering, Xidian University, Xi'an 710071, China; sxue@xidian.edu.cn
[2] Guangzhou Institute of Technology, Xidian University, Guangzhou 510555, China; yfyan530@163.com
[3] University of Chinese Academy of Sciences, Beijing 100049, China
[4] The 39th Research Institute of China Electronics Technology Group Corporation, Xi'an 710065, China
[5] Xinjiang Astronomical Observatory, Chinese Academy of Sciences, Urumqi 830011, China
Received 2023 March 29; revised 2023 April 17; accepted 2023 April 26; published 2023 July 26

Abstract

Obtaining the wind load distribution on the telescope aperture is very important to estimate its influence and reduce the wind disturbance on the telescope system. The aperture of the radio telescope structure can be as large as 100 m and therefore, the uniform wind load on the aperture assumption is not suitable for the radio telescope with large aperture. In this paper, a gradient segments superposition method for calculating the wind load has been proposed. The proposed method has been constructed by combining two regional divisions. First, reflecting surface has been evenly divided in the altitudinal direction. Second, the reflecting surface has been divided into several uniform rings assuming that the wind load coefficient on different rings are different. For the 110 m aperture radio telescope, the wind load estimation results differ by 28%. After that, a structural dynamics model of telescope has been established and a fuzzy PID controller has been designed to reduce wind disturbance. The Root Mean Square Error of telescope pointing under wind disturbance has been reduced by 67.8%. It is suggested that the proposed wind load estimation method has lay a solid foundation for the design of the large telescope system under wind disturbance.

Key words: methods: analytical – methods: data analysis – methods: numerical – telescopes

1. Introduction

Radio telescope is an important tool for human to explore the universe and observe celestial bodies (Wielebinski 1970; Clark et al. 2023). With the continuous development of radio astronomy, the demand for "clear," "accurate" and "stable" radio telescopes is becoming more and more intense. Therefore, large aperture, high precision and high gain become the inevitable trend of the development of radio telescopes (Yan et al. 2022). At the same time, this puts a more demanding requirement on the pointing accuracy of radio telescopes. With the increase of the aperture, the upwind area of the radio telescope increases and the structural stiffness decreases, leading to the more significant influence of wind disturbance on the radio telescope (Zhang et al. 2017). In order to overcome the effect of wind load, engineers take a variety of measures. (1) The large millimeter-wave radio telescope (LMT 50 m) is equipped with actuators on the back of the reflecting surface (Hughes et al. 2020). (2) The 37 m aperture radio telescope at MIT's Haystack Observatory is fitted with a radome (Olmi & Mauskopf 1999). (3) The QiTai Telescope (QTT) 110 m aperture radio telescope, which is being prepared for construction, intends to adopt active wind field control technology to improve the wind field environment of the radio telescope site (Wang et al. 2019). (4) The US Deep Space Network (DSN) 70 m aperture radio telescope has improved the servo control system.

For very large aperture radio telescopes, measure (4) has been widely concerned by very large aperture radio telescope builders because of its low cost and remarkable effect. In order to restrain the disturbance caused by wind load, it is necessary to calculate the size of wind load and clarify the effect of wind load. Ralph C. Snel (Snel et al.2007) measured the rigid body motion of the antenna elevation structure by installing an accelerometer system on the Atacama Large Millimeter Array (ALMA) to study the dynamic performance of the antenna under operating conditions and the effect of wind (Gawronski 2004). But it can only measure low-frequency vibrations, which is not negligible for very large aperture radio telescopes. Ranka, Trupti identified the model of Green Bank Telescope (GBT), (Ranka et al. 2014) observed the performance of GBT servo system under wind disturbance, and developed a simplified model suitable for the controller (Trupti et al. 2016). However, it requires field measurement, which is

[6] Corresponding authors.

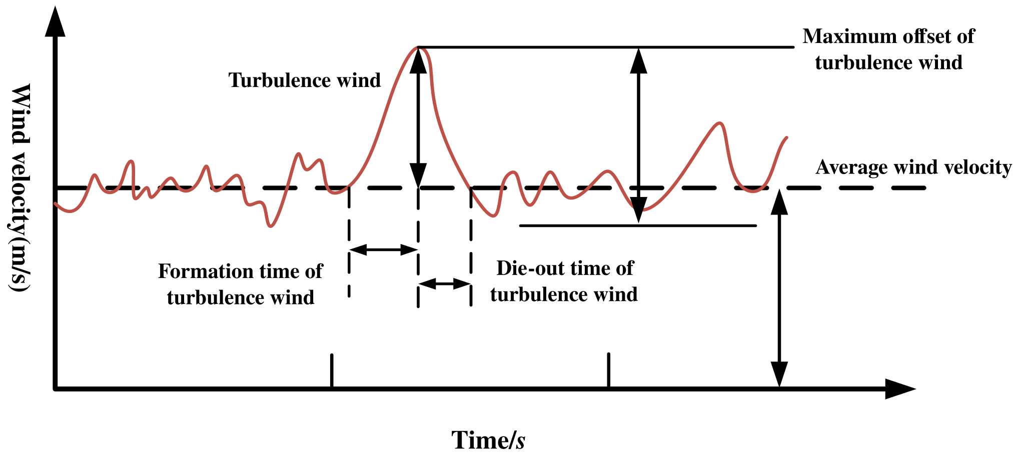

Figure 1. The composition of wind.

impossible for most researchers. Wodek Gawronski developed three wind models for simulating antenna servo error in order to study a more extensive wind load calculation method, but the accuracy was insufficient. Liu Yan studied the wind vibration characteristics of different types of reflectors and different working conditions through CFD simulation and wind tunnel tests (Liu et al. 2017). However, the structural flexibility and velocity gradient of the very large aperture radio telescope are not considered. After determining the influence of wind disturbance on a servo system, it is necessary to further design the anti-wind disturbance servo control system to suppress the interference brought by wind load. Gawronski Wodek improved the DSN 70 m radio telescope servo controller, developed the LQG(linear quadratic Gaussian control) control algorithm for 70 m antenna, and found that the LQG control algorithm can effectively suppress wind disturbance. By comparing PI (proportional integral control)-PI, PI-LQG, LQG-PI and LQG-LQG four control algorithms, it is found that LQG-LQG algorithm has the best control effect (Gawronski & Souccar 2005). Zaher M. Kassas derived the optimal control rate of the control system of Extremely large telescopes ELT, and found that H_2 and H_∞ had the best imaging performance in the case of wind disturbance (Zaher & Rober 2012). Tao Tang analyzed and compared the suppression effects of PI, LQG, DFF (disturbance feedforward control) and DOBC (disturbance observer control) on disturbance of different frequencies (Tang et al. 2019). Among them, DOBC has a great suppression ability on disturbance.

In view of the characteristics of high flexibility and long span of the reflector of a very large aperture radio telescope, a calculation method of the wind load on the reflector is proposed based on the exponential distribution of wind speed in the wind field of the program and site of the radio telescope structure, considering the different wind load coefficients and incoming wind speeds in different areas of the reflector. The structural dynamics model of radio telescope and servo motor is established to study the effect of wind load on servo control system. The fuzzy adaptive PID controller is designed for wind load disturbance to enhance the robustness of the control system, improve the pointing accuracy of the radio telescope and realize the high performance observation of the radio telescope.

2. Calculation Method of Mean Wind Load

Wind is the flow of air from a place of high pressure to a place of low pressure. As soon as the air flow meets the blockage of the structure, it forms a high pressure air curtain. The faster the wind moves, the more pressure it exerts on the structure. This will cause large deformation and vibration of the structure. So wind load is a factor that must be taken into account for a tall building like a large aperture radio telescope. In engineering, wind is usually divided into mean wind and fluctuating wind. The effects of wind loads on radio telescopes are studied mainly from the mean wind loads and turbulence wind loads. In this paper, we investigate and suppress the effect of average wind load on the pointing of radio telescope. The composition of wind is shown in Figure 1.

2.1. Traditional Calculation Method of Mean Wind Load

When the wind blows from the front toward the reflector of a radio telescope, there will be a pressure difference between the wind and leeward side of the reflector, causing the reflector to rotate. The reflection surface is subjected to the average wind, resulting in six components, such as resistance, side force, lift force, rolling moment, pitching moment and yawing moment. A diagram of the effect of a radio telescope on the average wind is shown in Figure 2. Here a_0o is the direction of wind speed, which is the wind axis and parallels to the horizontal plane, a_2o is the direction of the radio telescope, a_1o is the horizontal projection of a_2o.

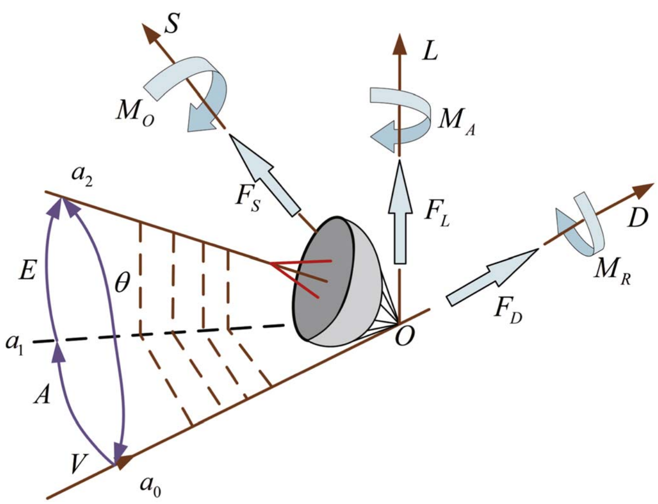

Figure 2. Diagram of mean wind action.

The average wind load calculation formula is obtained by deducing the basic formula in the mechanics of convection, and the six components of the average wind load can be obtained by Equation (1).

$$\begin{cases} F_D = C_L qA \\ F_S = C_S qA \\ F_L = C_L qA \\ M_R = C_{MR} qAD \\ M_O = C_{MO} qAD \\ M_A = C_{MA} qAD \\ q = \dfrac{1}{2}\rho V^2 \end{cases} \tag{1}$$

Where F_D is resistance, F_S is side force, F_L is lift force, M_R is rolling torque, M_O is pitching torque, M_A is yawing torque, C is the torque coefficient, q is dynamic pressure of the undisturbed flow, ρ is air density, V is average wind velocity, A is the diameter area of reflector, D is the diameter of the paraboloid.

The wind load coefficients under different working conditions were obtained by searching the data of wind tunnel experiments in China. The data of QTT 110 m aperture radio telescope in QiTai, Xinjiang were taken as an example to calculate the wind load under different working conditions. According to the geographical and climatic information of QiTai (Wang 2014), the average annual temperature of Qitai is 5.5°C, 278.65 Fahrenheit. The altitude is about 1760 m, and the atmospheric pressure is about 81.5 kPa. According to the air density calculation formula, the air density of the QiTai is about 1.02 $\mathrm{kg\,m^{-2}}$. According to the wind tower data, the average wind speed at 60 m of the platform site is 6.6 $\mathrm{m\,s^{-1}}$, and the dynamic pressure of the undisturbed flow is obtained $q = 22.2\ \mathrm{kg\,m^{-2}}$, $qA = 211015.72N$, $qAD = 23211728.97N$. Then the wind load force and torque of QTT can be obtained according to the above parameters. The specific data are shown in Figure 3.

2.2. Calculation of Mean Wind Load for Very Large Aperture Radio Telescope

For QTT, a full-mobile radio telescope of very large aperture, there is a large difference in wind speed between the top and the bottom, and a large difference in torque coefficient between the edge of the radio telescope and the center surface of the radio telescope. As a result, the method described in the above section has a large error and cannot accurately reflect the effect of wind load on the reflecting surface. Therefore, based on the high symmetry of the reflector of radio telescope, the reflector is divided into ring equipartition. Based on the exponential distribution of the site wind field with height, the reflecting surface is evenly divided every certain wind velocity gradient. The above two partitioning methods are jointly divided, and the specific partitioning is shown in Figure 4.

Figure 4 reflects the relationship between the wind velocity gradient and the zone radius of the reflecting surface. The wind velocity gradient is the vertical projection of the zone radius of the reflecting surface, which is specifically shown in Equation (2).

$$r_1 \cos\theta = z_1 \tag{2}$$

Here θ is the pitch angle, z_1 is the preset wind speed gradient. Then the height from the midpoint of the equivalent reflector to the ground is calculated. As shown in Equation (3).

$$h = F\sin\theta + h_0 \tag{3}$$

Here h is the height of the center of the equivalent aperture of the reflector, h_0 is frame height, F is the focal length of the reflector. Then the equivalent wind speed height of any partition is calculated. As shown in Equation (4)

$$z_m = \begin{cases} h + \dfrac{2m-1}{2} z_1,\ m > 0 \\ h + \dfrac{2m+1}{2} z_1,\ m < 0 \end{cases} \tag{4}$$

Here z_m is equivalent height of reflector zone (Q_{lm}), where l is the first number of the partition. The reflecting surface is evenly divided into rings, and l indicates that the partition is in the l circle. m is the second number of the partition, m represents the distance between the zone and the antenna center with m wind speed gradients. In engineering, exponential law is generally used for simulation. The relationship between wind speed at any height and terrain is shown in Equation (5).

$$V = V_0 \left(\frac{z_m}{z_r}\right)^{\beta} \tag{5}$$

Here z_r is reference height, where V_0 is average wind speed at reference height, β is wind velocity profile index and it

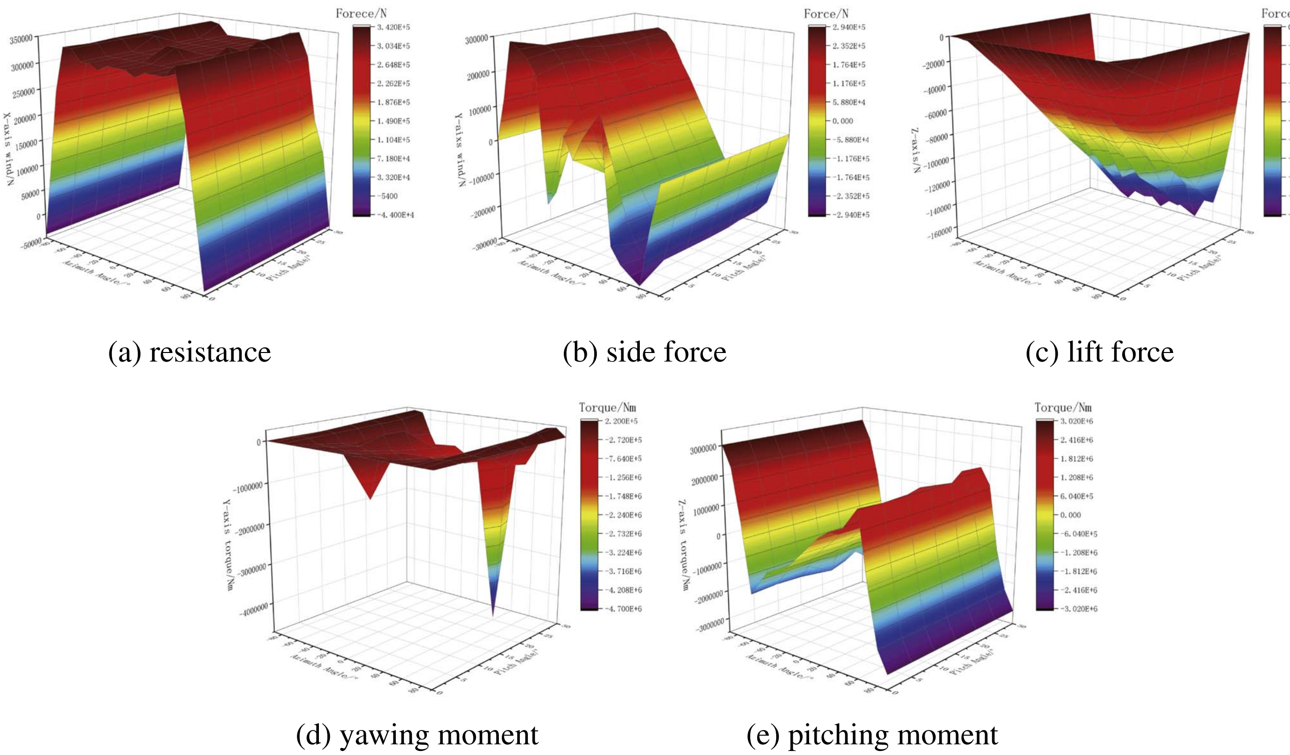
(a) resistance (b) side force (c) lift force

(d) yawing moment (e) pitching moment

Figure 3. Wind power and wind torque under different working conditions.

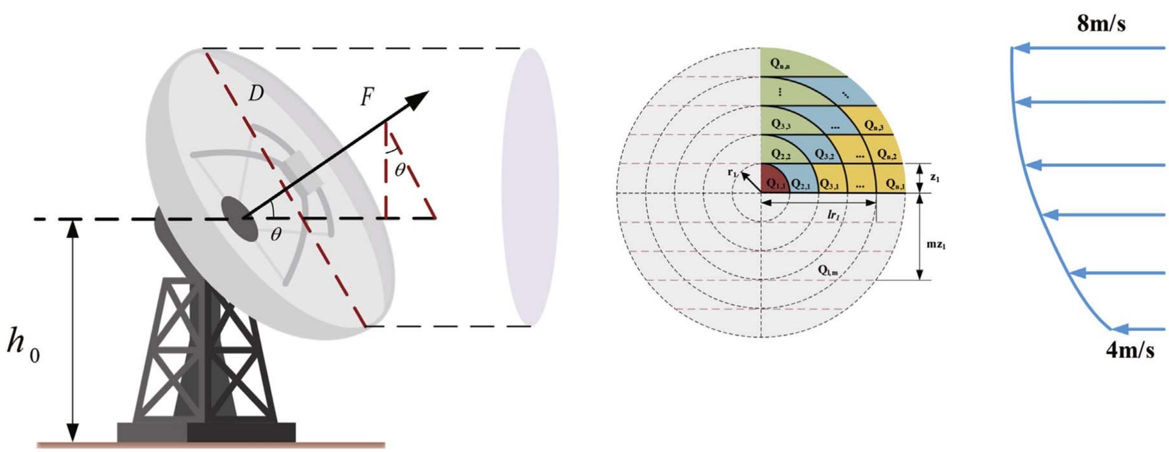

Figure 4. Schematic diagram of wind acting on a radio telescope and panel partition.

depends on the topography of the site. The expression of wind power in any partition can be obtained by integrating the above formulas, as shown in Equation (6).

$$F_{lm} = \frac{1}{2}\alpha_{lm} c_{lm} \rho V_0^2 \left(\frac{z_m}{z_1}\right)^{2\beta} l^2 \left(\frac{z_1}{cos\theta}\right)^2 \tag{6}$$

Here F_{lm} is the wind torque applied to any partition (Q_{lm}), α_{lm} is proportionality coefficient, the value is the ratio of the area of the partition to the full area. c_{lm} is reflecting surface wind load coefficient, ρ is air density, z_1 is the reference height of the wind speed gradient, which is generally selected as 10 m. Different calculation methods are used for different partitions, such as Equations (7)–(10). Equations (11) and (12) are used to calculate the total wind force and wind moment on the reflecting surface of the radio telescope.

Table 1
Ratio Coefficient of Each Partition

Q_{lm}	$m=1$	$m=2$	$m=3$	$m=4$	$m=5$	$m=6$	$m=7$	$m=8$	$m=9$	$m=10$	$m=11$
l=1	0.25	\	\	\	\	\	\	\	\	\	\
$l=2$	0.0897	0.0978	\	\	\	\	\	\	\	\	\
$l=3$	0.0364	0.0477	0.0548	\	\	\	\	\	\	\	\
$l=4$	0.0202	0.0223	0.0309	0.0361	\	\	\	\	\	\	\
$l=5$	0.0128	0.0136	0.0155	0.0221	0.026	\	\	\	\	\	\
$l=6$	0.0089	0.0092	0.01	0.0116	0.0168	0.0199	\	\	\	\	\
$l=7$	0.0065	0.0067	0.0071	0.0077	0.0091	0.0133	0.0159	\	\	\	\
$l=8$	0.005	0.0051	0.0053	0.0056	0.0062	0.0074	0.0109	0.013	\	\	\
$l=9$	0.0039	0.004	0.0043	0.0043	0.0046	0.0052	0.0062	0.0092	0.0109	\	\
$l=10$	0.0032	0.0032	0.0033	0.0034	0.0036	0.0039	0.0044	0.0053	0.0078	0.0093	\
$l=11$	0.0026	0.0027	0.0027	0.0028	0.0029	0.0031	0.0034	0.0038	0.0045	0.0068	0.0081

When l=$|m|$=1,

$$\alpha_{lm} = \frac{1}{4} \tag{7}$$

When $l = |m| \neq 1$,

$$\alpha_{lm} = \frac{l^2\arccos(\frac{l-1}{l}) - (l-1)\sqrt{2l-1})}{2\pi l^2} \tag{8}$$

When l-$|m| > 1$,

$$\begin{aligned}\alpha_{lm} = &\left(\frac{1}{2\pi l^2}(|m|\ \sqrt{l^2 - m^2}\ + (|m| - 1))\right.\\ &\times \sqrt{(l-1)^2 - (m-1)^2}\ - |m|)\sqrt{(l-1)^2 - m^2}\\ &+ (l-1)^2[\arccos\left(\frac{|m|-1}{l}\right) + \arccos\left(\frac{|m|}{l-1}\right)\\ &- \arccos\left(\frac{|m|-1}{l-1}\right)\\ &- (|m|-1)\sqrt{l^2 - (m-1)^2}\\ &\left. + (2l-1)\arccos\left(\frac{|m|-1}{l}\ - \arccos\left(\frac{|m|}{l}\right)\right)\right)\end{aligned} \tag{9}$$

When l-$|m|$=1,

$$\begin{aligned}\alpha_{lm} = &\left(\frac{1}{2\pi l^2}(|m|\ \sqrt{l^2 - m^2}\right.\\ &+ (|m| - 1))\sqrt{(l-1)^2 - (m-1)^2}\\ &+(l-1)^2[\arccos\left(\frac{|m|-1}{l}\right) - \arccos\left(\frac{|m|}{l}\right)\\ &- \arccos\left(\frac{|m|-1}{l-1}\right)\\ &\left.-|m-1|\ \sqrt{l^2 - (m-1)^2}\ + (2l-1)\arccos\left(\frac{|m|-1}{l}\right)\right)\end{aligned} \tag{10}$$

$$F = \sum_{l=1}^{l=n}\sum_{m=1}^{m=n} F_{lm} + \sum_{l=-n}^{l=-1}\sum_{m=-n}^{m=-1} F_{lm} \tag{11}$$

$$\begin{aligned}F = &\sum_{l=1}^{l=n}\sum_{m=1}^{m=n} F_{lm}\frac{lr_1\sqrt{4P^2 + D^2}}{D}\\ &- \sum_{l=1}^{l=n}\sum_{m=-n}^{m=-1} F_{lm}\frac{lr_1\sqrt{4P^2 + D^2}}{D}\end{aligned} \tag{12}$$

Here F is the total wind force on the reflecting surface, M is the total wind torque on the reflecting surface, D is the diameter of the reflecting surface, and P is focal diameter of the reflector.

The QTT 110 m radio telescope is also taken as an example below. The focal aspect ratio (F/D) is equal to 0.3, the antenna pitch angle is 0°, its focal length is 33 m, and the height from the midpoint of the reflector to the ground of the radio telescope is 60 m. Qitai site topography belongs to B type landform (He et al. 2021), the wind speed profile index is 0.16. Taking the reference height as 5 m and the wind speed at the reference height as 2 m s^{-1}, the antenna reflector can be divided into 22 horizontal zones, the height of each zone is 5 m, and there are 264 zones in total. The proportional coefficients of each partition can be obtained by putting the data into the formula, as shown in Table 1. The wind force received by each zone and the wind force at each height of the reflecting surface are shown in Figure 5.

Five different aperture telescopes, 110, 80, 50, 30 and 10 m, are used to estimate the wind load on their surface. As it can be seen from Figure 6, there are differences between the two estimation methods, and the gap between calculation results increases with the increasing aperture. Table 2 presents the specific wind load calculation result of five different aperture telescopes. When the aperture increases, the error caused by the traditional calculation method will become more obvious. The method proposed in this paper will provide more accurate wind load estimation.

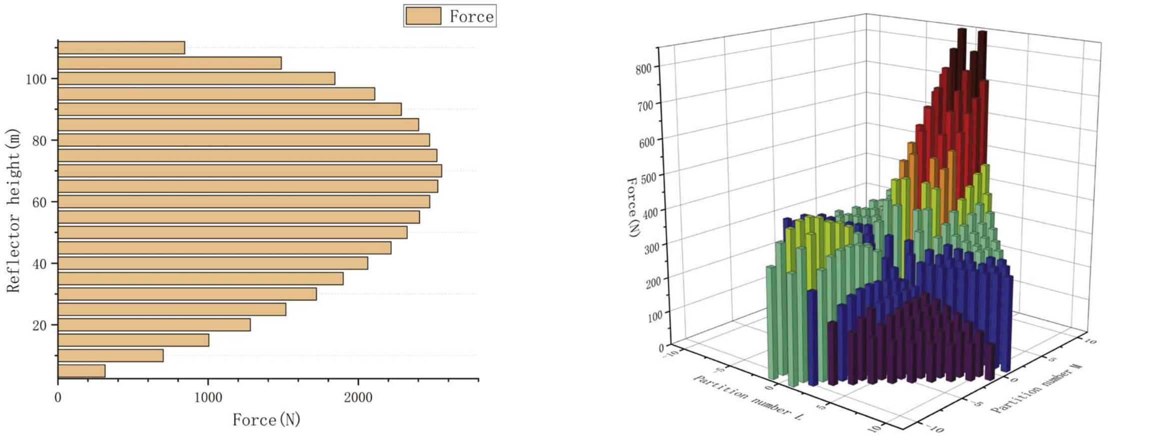

(a) Wind load at each height of the reflector (b) Wind load in each zone of the reflecting surface

Figure 5. Wind load distribution on reflecting surface.

3. Large Radio Telescope System Dynamic Model

In order to eliminate the influence of wind disturbance on servo direction through servo control system, the system control model of the large radio telescope must be established. In this section, considering that the wind load will cause the structural vibration of the radio telescope, the structural dynamics model of the large radio telescope will be established.

The radio telescope servo control system is mainly divided into two parts: system modeling and control algorithm. System modeling is the basis of the servo control system, the accurate control system model will directly significantly improve the pointing accuracy of radio telescope, but also greatly facilitate the design of control system. The servo direction of a fully mobile radio telescope can be divided into the azimuth direction and pitch direction. The radio telescope controller consists of two independent subsystems: the azimuth control subsystem and pitch control subsystem. The radio telescope servo system generally adopts three-ring control, which consists of current ring, speed ring and position ring from inside to outside, as shown in Figure 7.

The movable telescope has a large reflecting surface, which will show a considerable degree of flexibility in the working process. The structure of the radio telescope is also affected by the dynamic load. Therefore, when the control model of the radio telescope is established, the radio telescope cannot be regarded as a rigid body, but its vibration should be considered. In this paper, a dynamic model of radio telescope structure is established to study the internal force and displacement of the structure under dynamic load. The equivalent model of the radio telescope structure is shown in Figure 8.

In this paper, Lagrange equation and Newton's second law are used to solve the two equations simultaneously to get the

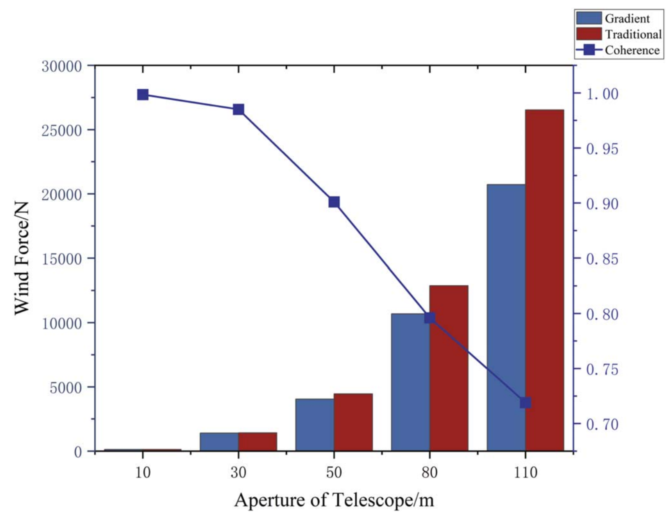

Figure 6. Two methods of wind estimate.

Table 2
Two Methods of Wind Estimate

	10 m	30 m	50 m	80 m	110 m
Gradient	127.3N	1395.5N	4049.7N	10689.8N	20718.2N
Traditional	127.1N	1417.0N	4450.1N	12872.3N	26524.9N
Incoherence	0.16%	4.12%	9.89%	20.41%	28.03%

mathematical model of the radio telescope. As shown in Equations (13) through (18).

$$M\ddot{q} + e\dot{q} + kq = Q(\dot{q}, q, u, t) \tag{13}$$

Here M is mass matrix, e is damping matrix, k is stiffness matrix, Q is matrix of inputs, q is the vector of generalized

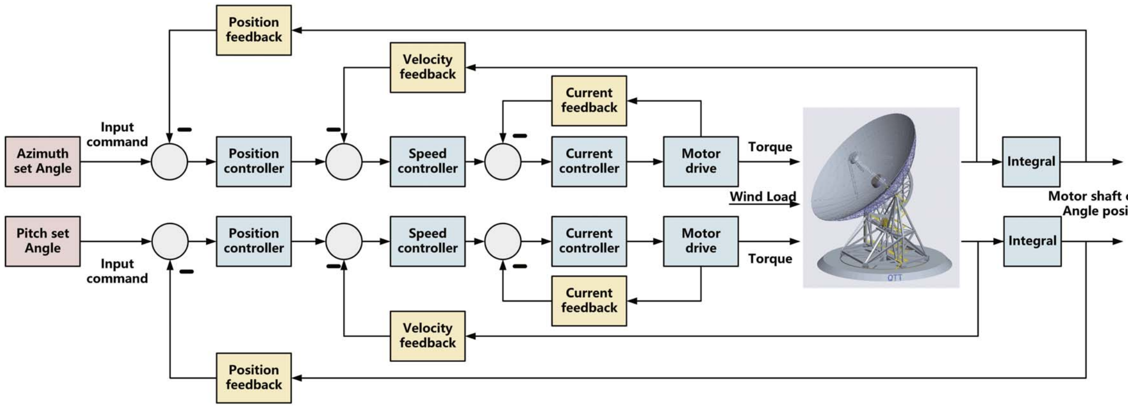

Figure 7. Radio telescope servo system block diagram.

coordinates, u is the vector of inputs, t is time variable.

$$\frac{d}{dt}\left(\frac{\partial L}{\partial \dot{q}_i}\right) - \frac{\partial L}{\partial \dot{q}_i} + \frac{\partial D_d}{\partial \dot{q}_i} = Q_i,\ i = 1,\ 2, \ldots n \quad L = E_k - E_p \tag{14}$$

Here q_i are the generalized coordinates or degrees of freedom of the system, Q are the generalized forces applied to each subsystem i, E_k is kinetic energies, E_p is potential energies, D_d is the dissipator co-content, L is the Lagrangian.

$$\begin{aligned} E_k = \frac{1}{2}J_d\dot{\theta_d}^2 + \frac{1}{2}J_b\dot{\theta_b}^2 + \frac{1}{2}NJ_t\dot{\theta_t}^2 \\ + \frac{1}{2}NJ_w(R\dot{\theta})^2 + \frac{1}{2}NJ_m(\dot{\theta}_m)^2 \end{aligned} \tag{15}$$

$$\begin{aligned} E_p = \frac{1}{2}K_s(\theta_d - \theta_b)^2 + \frac{1}{2}NK_b(\theta_b - \theta_t)^2 \\ + \frac{1}{2}NK_m(R\theta_t - \theta_m)^2 \end{aligned} \tag{16}$$

$$\begin{aligned} D_d = \frac{1}{2}R_s(\dot{\theta}_d - \dot{\theta}_b)^2 + \frac{1}{2}NB_b(\dot{\theta}_b - \dot{\theta}_t)^2 \\ + \frac{1}{2}NB_m(R\dot{\theta}_t - \dot{\theta}_m)^2 \end{aligned} \tag{17}$$

$$Q = \begin{bmatrix} 1 & 0 \\ 0 & 0 \\ 0 & 0 \\ 0 & N \end{bmatrix} \begin{bmatrix} T_W \\ T_M \end{bmatrix} \tag{18}$$

Where $\theta_d(t)$ is dish angular position, $\theta_b(t)$ is base (lower structure) angular position, $\theta_t(t)$ is truck angular position, $\theta_m(t)$ is motor shaft angular position at the gearbox output, T_w is aerodynamic torque applied by the wind on the dish and structure, T_m is equivalent torque applied by the four motors of each truck, θ_w is truck wheel angular position, $\theta_w = \theta_t(r_b/r_w)$), r_b is radius of the arm between the lower structure and each truck, r_w is radius of the equivalent truck wheel, R is radius rate, $R = r_b/r_w$. The parameters of the radio telescope structure (Garcia-Sanz 2017) are shown in Table 3.

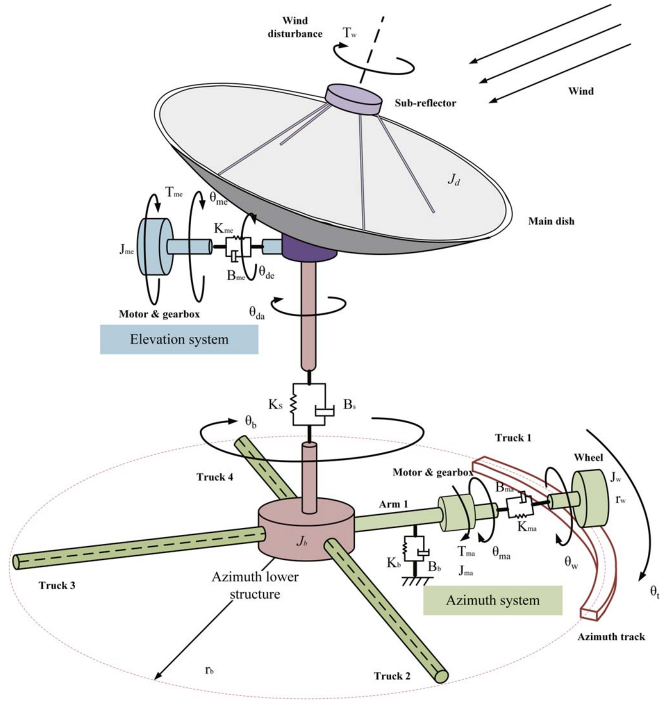

Figure 8. Equivalent model of azimuth structure for radio telescope.

Motor position ($\theta(t)$) is controlled by motor armature voltage(v_a). Their relationship is shown in Equation (19).

$$v_a = L_a\frac{d_{i_o}}{dt} + R_a i_o + k_i\frac{d\theta_m}{dt} \tag{19}$$

Here L_a is armature inductance, R_a is armature resistance, k_i is current feedback coefficient, i_o is motor current.

Table 3
Parameters of Structural Dynamics Model

Symbol	Physical Meaning	Numerical Value (unit)
J_d	moment of inertia of dish, feed arm, and upper structure	102×10^6 kg m^2
J_b	moment of inertia of lower structure	34.3×10^6 kg m^2
J_t	moment of inertia of each truck	3.43×10^6 kg m^2
J_w	moment of inertia of each equivalent truck wheel	426 kg m^2
J_m	moment of inertia of each equivalent motor with its brake, gearbox, and shaft	517.56 kg m^2
K_s	upper structure torsional stiffness coefficient	$1.9731 \times 10^9 N$ m^{-1}
B_s	upper structure torsional damping coefficient	$4.4862 \times 10^6 Ns$ m^{-1}
K_b	one arm torsional stiffness coefficient	$94.9 \times 10^6 N$ m^{-1}
B_b	one arm torsional damping coefficient	$3.1249 \times 10^5 Ns$ m^{-1}
K_m	one motor shaft torsional stiffness coefficient	$1.6851 \times 10^5 N$ m^{-1}
B_m	one motor shaft torsional damping coefficient	$274.89 Ns$ m^{-1}
L_a	motor inductance	$0.007H$
R_a	motor resistance	0.52Ω
K_i	motor current feedback	$0.85V$ A^{-1}
K_t	motor torque coefficient	$0.89Nm$ A^{-1}
N	number of axes	4

T_m is proportional to the current of the motor. k_i is motor torque coefficient.

$$T_m = k_i i_o \tag{20}$$

The motor torque is in equilibrium with the remaining torque acting on the rotor, T is output torque. Therefore,

$$J_m \ddot{\theta}_m = k_i i_o + T \tag{21}$$

According to the above equations, the spatial state equation and transfer function with motor torque and wind disturbance dynamic moment as input and azimuth-pitch axis as output are obtained. The following is an analysis of the established model, as shown in Figure 9. The four parameters of amplitude margin, phase margin, amplitude crossing frequency (cutoff frequency) and phase crossing frequency of the system were calculated respectively to analyze the open-loop characteristics of the system.

When the input is motor torque and the output is azimuth axis angle, the transfer function is p_{11}; when the input is motor torque and the output is pitch shaft angle, the transfer function is p_{21}; when the input is wind disturbance torque and the output is azimuth axis angle, the transfer function is p_{12}; when the input is wind disturbance torque and the output is pitch axis angle, the transfer function is p_{22}. The four parameters of amplitude margin, phase margin, amplitude crossing frequency (cutoff frequency) and phase crossing frequency are obtained respectively. This shows that the control system of the telescope is very unstable, and it needs to be improved by adding a controller to improve its stability and control precision.

4. Fuzzy PID Control that Against Wind Disturbance

PID control is the most widely used control, and is used by a large number of radio telescopes. Its performance has been tested in the real world, so PID control is considered. In addition, the PID control algorithm has low requirements on model accuracy, and it is easy to adjust parameters, so it can be easily applied to the actual situation. Further considering that the PID control performance may not meet the 100 m level radio telescope, we add fuzzy theory on the basis of the PID control algorithm to adjust the parameters of the PID control algorithm. The results show that the fuzzy adaptive PID control algorithm can obviously improve the control effect.

Convert the resulting controlled object into a transfer function, as shown in Equation (22).

$$\mathrm{sys} = \frac{0.2456s^6 + 0.1065s^5 + 256.9s^4 + 54.43s^3 + 20690s^2 + 282.3s + 49270}{s^8 + 75.25s^7 + 6281s^6 + 322700s^5 + 8.733 \times 10^6 s^4 + 3.495 \times 10^7 s^3 + 8.467 \times 10^8 s^2 + 1.179 \times 10^{10}} \tag{22}$$

The plant can be controlled by speed-position loop. PI control is used for speed loop, and PI and fuzzy adaptive PID control are used for position loop respectively.

4.1. Design of Fuzzy Adaptive PID Controller

Fuzzy adaptive PID control is a kind of control method that makes use of fuzzy logic and certain fuzzy rules to optimize the PID parameters in real time. It can adjust the PID parameters according to the system deviation and the change of the deviation to achieve better control effect. Fuzzy adaptive PID control includes fuzzy, fuzzy rule determination, defuzzy and other components, the specific schematic diagram is shown in Figure 10.

Traditional PID controller has become the most commonly-used control mode in industry because of its advantages of simple structure, easy implemefuzntation and reliable operation. Parameters need to be adjusted during controller design. Proportional gain (P) is used to improve the response speed and force. When the response is less than the ideal output or too

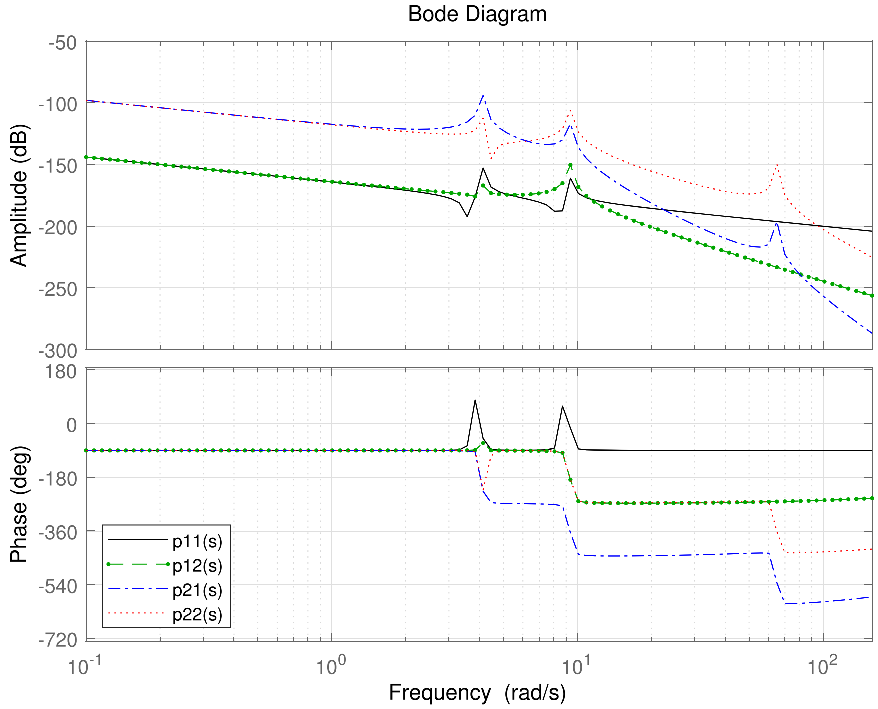

Figure 9. Bode diagram.

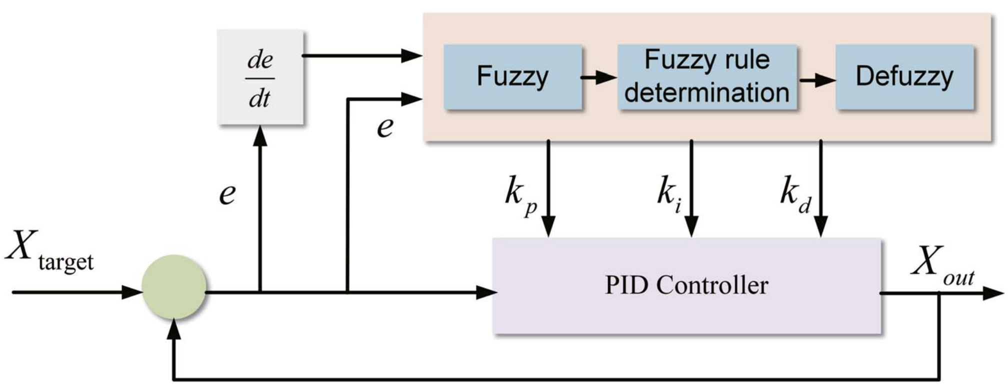

Figure 10. Principle of fuzzy adaptive PID.

slow, the proportional gain needs to be increased, but when the proportional gain is too large, it will produce too large oscillation. Integral gain (*I*) is used to eliminate steady-state error and improve accuracy, and also to increase response speed. However, too large will cause oscillation. Differential gain (*D*) is used to suppress over harmonic oscillations and prevent abrupt changes in the system. Parameters *P, I* and *D* are adjusted according to the deviation between the actual output and the ideal output. Based on the above experience, this paper designs fuzzy rules for the radio telescope servo control system, as shown in Figure 11. Figure (a), (b) and (c) are fuzzy rules of proportional coefficient, integral coefficient and differential coefficient of PID control respectively, and Figure (d), (e) and (f) are three-dimensional image display of fuzzy rules respectively. Here, PB is superplot, PM is median, PS is positive small, Z is zero, NS is negative small, NM is negative medium, NB is negative large, and their respective membership functions of fuzzy subsets on the discussion domain are triangular.

4.2. Simulation and Analysis

The radio telescope servo system is simulated. By comparing the results obtained by two different calculation methods, there

Kp		*Ec* NB	NM	NS	Z	PS	PM	PB
E	NB	PB	PB	PM	PM	PS	Z	Z
	NM	PB	PB	PM	PS	PS	Z	NS
	NS	PM	PM	PM	PS	Z	NS	NS
	Z	PM	PM	PS	Z	NS	NM	NM
	PS	PS	PS	Z	NS	NS	NM	NM
	PM	PS	Z	NS	NM	NM	NM	NB
	PB	Z	Z	NM	NM	NM	NB	NB

(a) Proportional fuzzy rule

Ki		*Ec* NB	NM	NS	Z	PS	PM	PB
E	NB	NB	NB	NM	NM	NS	Z	Z
	NM	NB	NB	NM	NS	NS	Z	Z
	NS	NM	NM	NS	NS	Z	PS	PS
	Z	NM	NM	NS	Z	PS	PM	PM
	PS	NM	NS	Z	PS	PS	PM	PB
	PM	Z	Z	PS	PS	PM	PB	PB
	PB	Z	Z	PS	PM	PM	PB	PB

(b) Integral fuzzy rule

Kd		*Ec* NB	NM	NS	Z	PS	PM	PB
E	NB	PS	NS	NB	NB	NB	NM	PS
	NM	PS	NS	NB	NM	NM	NS	Z
	NS	Z	NS	NM	NM	NS	NS	Z
	Z	Z	NS	NS	NS	NS	NS	Z
	PS	Z	Z	Z	Z	Z	Z	Z
	PM	PB	PS	PS	PS	PS	PS	PB
	PB	PB	PM	PM	PM	PS	PS	PB

(c) Differential fuzzy rule

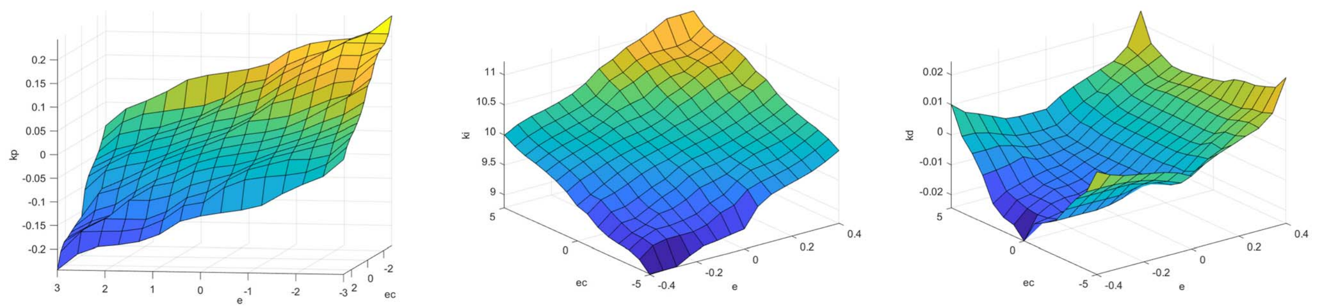

(d) Proportional rule surface (e) Integral rule surface (f) Differential rule surface

Figure 11. Fuzzy rule.

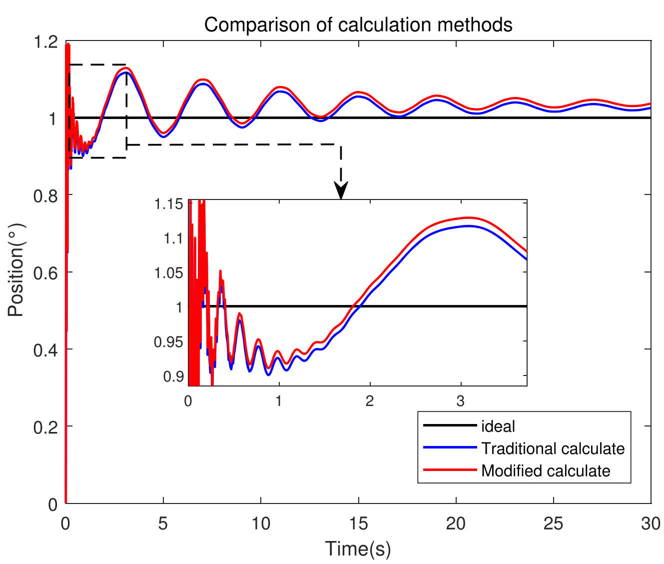

Figure 12. Position tracking.

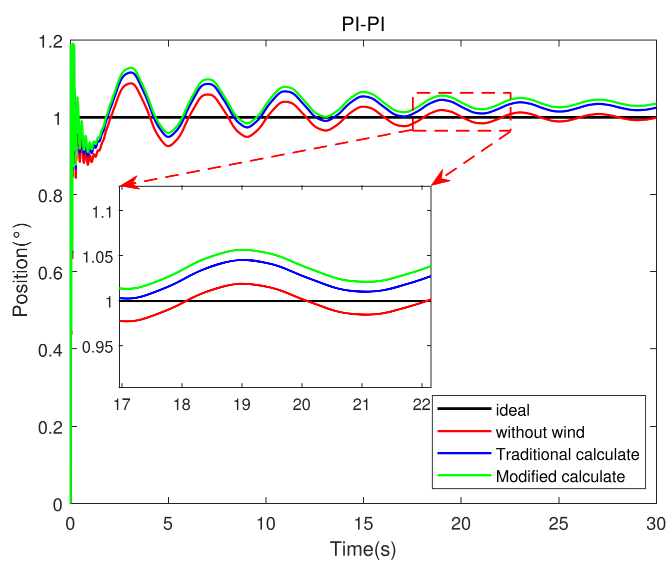

Figure 13. Position tracking curve of PI–PI in windy and non-windy conditions.

Table 4
Position Tracking Error Comparison

	Mean(°)	Maximum Tracking Error(°)	Root Mean Square Error(°)
Traditional calculation method	1.0231	0.1838	0.0429
New calculation method	1.0342	0.1909	0.0500
difference	0.0111	0.0071	0.0071

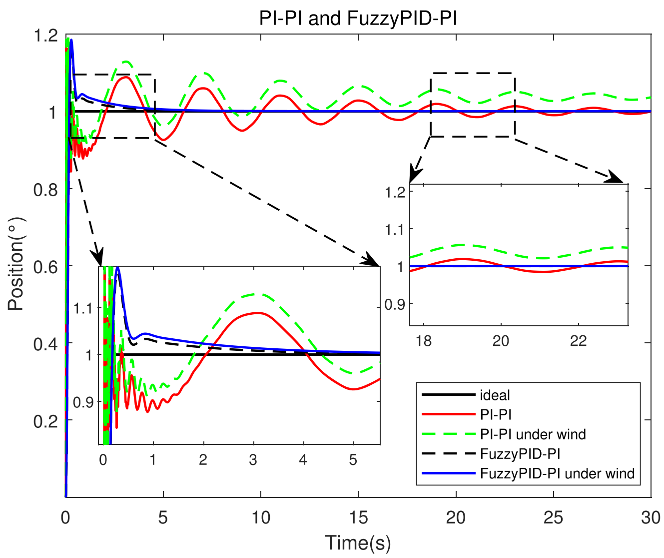

Figure 14. Position tracking curve of Fuzzy PID-PI and PI-PI.

Table 5
PI-PI Position Tracking Error under Wind and No Wind

	Mean(°)	Maximum Tracking Error(°)	Root Mean Square Error(°)
No wind	0.9973	0.1754	0.0353
Traditional calculation method	1.0231	0.1838	0.0429
New calculation method	1.0342	0.1909	0.0500

Table 6
Fuzzy PID-PI and PI–PI Position Tracking Error

	Mean (°)	Maximum Tracking Error(°)	Root Mean Square Error(°)
No wind with PI	0.9973	0.1754	0.0353
No wind with Fuzzy	1.0026	0.1733	0.0138
Reduce	/	1.2%	60.9%
Wind with PI	1.0342	0.1909	0.0500
Wind with Fuzzy	1.0044	0.1850	0.0161
Reduce	/	3.19%	67.8%

are differences between the two curves, that is, different calculation methods will affect the compensation effect of wind load. In addition, due to the high accuracy requirement of the very large aperture radio telescope, the wrong calculation method will lead to the wrong compensation method, resulting in a large pointing error. The position tracking curve caused by the two calculation methods is shown in Figure 12, and the calculated mean value, maximum tracking error and root mean square error are shown in Table 4.

As shown in Figure 13, the control effect of PI–PI controller (the controller of speed loop and position loop adopts PI controller) is compared in windy condition and no windy condition. It can be seen from the curves in the figure that the average wind load will cause errors to the pointing of the radio telescope, and the two calculation methods have different effects on the pointing. As shown in Table 5, the mean value, maximum tracking error and root mean square error of position tracking in two cases are listed.

As shown in Figure 14, the control effects of PI–PI controller and Fuzzy PID-PI (position ring adopts fuzzy adaptive PID controller and position ring adopts PI controller) are respectively compared under the condition of wind and no wind. It can be seen from the curve in the figure that the fuzzy adaptive PID controller can obviously improve the pointing error of the radio telescope, and the root mean square error is greatly reduced. As shown in Table 6, the position tracking errors of the two control algorithms are compared.

5. Conclusion

For the very large aperture radio telescope, its servo controller needs better control performance and wind disturbance suppression ability. To reduce wind disturbance, it is necessary to study the nature of wind, the size of wind disturbance and the action mechanism of wind disturbance on the radio telescope. After studying these basic contents, it is necessary to continue to study wind disturbance control for wind load. In previous studies, the wind load calculation method for the reflector of a very large aperture radio telescope is the same as that for small and medium aperture radio telescopes. However, due to the differences in wind load coefficient between different areas of the very large aperture radio telescope reflector, and the very large span of the reflector, the wind speed difference between the top area and the bottom area of the reflector is nearly two times, and the wind speed difference is nearly four times, so the traditional wind load calculation method cannot meet the needs of the very large aperture radio telescope.

In this paper, a calculation method of wind load on reflecting surface is obtained based on the distribution characteristics of wind load and the structure characteristics of reflecting surface. Then, the action mechanism of wind load on the radio telescope servo control system is defined. Finally, a fuzzy adaptive PID controller is designed. To improve the pointing accuracy of very large aperture radio telescope under wind disturbance. In this paper, the theoretical model of the radio telescope is established, and then the pointing and tracking curves of the PI–PI controller and Fuzzy PID-PI controller are simulated respectively under two conditions of wind and no wind. The results show that the wind load has a great influence on the pointing accuracy of the very large aperture radio telescope. At the same time, the fuzzy adaptive PID controller can obviously improve the control performance of the servo system. The wind load calculation method has not been tested in this paper, but it can provide some reference for the design of the wind disturbance resistance servo control system of a very large aperture radio telescope.

Acknowledgments

This work was supported by the National Key Research and Development Program of China under No. 2021YFC2203600, the National Natural Science Foundation of China under Nos. 52005377 and 52275268, the National Defense Basic Scientific Research Program of China under No. JCKY2021210B007, Wuhu and Xidian University Special Fund for Industry-University-Research Cooperation under No. XWYCXY-012021012, Youth Innovation Team of Shaanxi Universities under No. 201926.

References

Clark, C. J., Kerr, M., Barr, E. D., et al. 2023, NatAs, 7, 451
Garcia-Sanz, M. 2017, Robust Control Engineering: Practical QFT Solutions (1st ed.; Boca Raton, FL: CRC Press), 365
Gawronski, W., Ahlstrom, H., & Bernardo, A. 2004, IAST, 43, 597
Gawronski, W., & Souccar, K. 2005, IAPM, 47, 41
He, F. L., Xu, Q., Wang, N., et al. 2021, ChA&A, 45, 118
Hughes, D. H., Schloerb, F. P., Aretxaga, I., et al. 2020, Proc. SPIE, 11445, 1144522
Liu, Y., Qian, H. L., Fan, F., et al. 2017, Adv. Steel Constr., 13, 1–29
Olmi, L., & Mauskopf, P. D. 1999, RaSc, 34, 733
Ranka, T., Garcia-Sanz, M., Weadon, T., & Ford, J. 2014, Proc. SPIE, 9145, 914554
Snel, R. C., Mangum, J. G., & Baars, J. W. M. 2007, IAPM, 49, 84
Tang, T., Niu, S. X., Ma, J. G., et al. 2019, Opto. Electron. Adv., 2, 10
Trupti, M. R., Mario, G., & Arthur, H. S. 2016, JATIS, 2, 014001
Wang, C. S., Wang, X. Q., Xu, Q., et al. 2019, SCPMA, 49, 099515
Wang, N. 2014, SCPMA, 44, 783
Wielebinski, R. 1970, Natur, 288, 507
Yan, Y. F., Wang, C. S., Li, S., et al. 2022, SCPMA, 52, 129501
Zaher, M. K., & Rober, H. B. 2012, Optimal H2 and H? Control of Extremely Large Segmented Telescopes in AIAA Guidance, Navigation, and Control Conf. (Minneapolis, MN: AIAA)
Zhang, J., Huang, J., Zhou, J., et al. 2017, IEEE Trans. Control Syst. Technol., 25, 1912